

High-Resolution Optical and Near-Infrared Images of the FS Tauri Circumbinary Disk*

Tomonori HIOKI¹, Yoichi ITOH¹, Yumiko OASA², Misato FUKAGAWA³, and Masahiko HAYASHI⁴

¹*Graduate School of Science and Technology, Kobe University, 1-1 Rokkodai, Nada, Kobe 657-8501
yitoh@kobe-u.ac.jp*

²*Faculty of Education, Saitama University, 255 Shimookubo, Sakura, Saitama, Saitama 338-0825*

³*Graduate School of Science, Osaka University, 1-1 Machikaneyama-cho, Toyonaka, Osaka 560-0043*

⁴*Graduate School of Science, The University of Tokyo, 7-3-1 Hongo, Bunkyo, Tokyo 113-0033*

(Received 2000 December 31; accepted 2001 January 1)

Abstract

We present an H -band image of FS Tauri, a $0''.2$ -separated classical T Tauri binary system, taken with the Coronagraphic Imager with Adaptive Optics (CIAO) on the Subaru Telescope. This new image, combined with Hubble Space Telescope / Advanced Camera for Surveys (HST/ACS) F606W-band polarimetric images, shows that the binary has complicated circumbinary features, including a circumbinary disk, western and eastern arm-like structures, and two cavities at the northeast and southwest. The circumbinary disk is 630 AU in radius and the southeast side of the disk is bright in the H -band. The brightness ratio (southeast/northwest) is 1.6 ± 0.4 . A single Rayleigh-like scattering model indicates that the disk is inclined by 30° to 40° and that the southeast side corresponds to the near side along our line of sight. The H -band surface brightness of the southeast side decreases as $r^{-1.9 \pm 0.1}$ from 15.2 mag arcsec⁻² to 16.8 mag arcsec⁻². The outer portion of the disk is possibly more flared than its inner portion. The weak centro-symmetric polarization pattern and redder F606W– H color (4.2 ± 0.2 mag) of the southeast side are probably caused by multiple scattering events from the dust grains associated with the binary. The F606W-band image shows the bright northwest side of the disk in contrast with the H -band image. The F606W– H color of the northwest side is between 1.7 mag and 3.0 mag. We consider that Haro 6-5 B (FS Tauri B), $20''$ away, produces the neutral scattered light from the northwest side. This idea is supported by the polarization pattern of the northwest side, which is centro-symmetric with respect to Haro 6-5 B. The arms appear to encompass the western and eastern cavities, suggesting that the arms + cavity systems are created by a bipolar outflow from the binary. However, the direction of this outflow is inconsistent with that of outflows inferred from the

circumbinary disk model. These differences may arise from misalignment between the circumbinary disk and the circumstellar disks. Another mechanism forming the arms + cavity systems is considered to be the inhomogeneous density distribution of materials in the circumbinary disk.

Key words: star: individual (FS Taurus) — star: pre-main sequence — techniques: high angular resolution

1. Introduction

Many studies have showed that the majority of young stars (≤ 1 Myr) are associated with various circumstellar structures, such as envelopes, protoplanetary disks, and/or bipolar outflows. The disks are composed of gas and dust, the possible birthplaces of planets. The bipolar outflow creates a cavity in the envelope. The cavity allows optical and near-infrared (NIR) radiation to escape and illuminate an extended reflection nebula. These circumstellar features have been directly revealed using ground-based telescopes with adaptive optics (AO) and the *Hubble Space Telescope* (*HST*).

A significant number of young stars appear in binary systems. NIR imaging surveys show multiplicity rates of 29 – 37% for Class I proto-stars in the ρ Ophiuchi molecular cloud (separation < 2000 AU; Haisch et al. 2002, 2004; Duchêne et al. 2004). This rate is quite high, despite the relatively poor sensitivity at the small projected separations (< 110 AU). Some mechanisms are proposed for the formation of protobinaries, in which the core fragmentation process is important (e.g., Boss 2002). In the standard core fragmentation scenario, a rotational and magnetic cloud core fragments into multiple dense objects and then a proto-binary is formed. The semi-major axis of the binary is determined by the initial core properties, especially by the magnetic and rotational energies and the angular momentum (Machida et al. 2008).

In the more evolved stage (Class II or classical T Tauri stars), binary systems have two kinds of protoplanetary disks: circumstellar disks associated with each star and ring-shaped circumbinary disks around the binary systems (Artymowicz & Lubow 1994, 1996). The sizes of the circumbinary disks and circumstellar disks depend on the binary system's semimajor axis, eccentricity, and mass ratio (Artymowicz & Lubow 1996; Armitage et al. 1999). Several observations have detected scattered light from the circumbinary disks using optical and NIR imaging/polarimetric methods, for instance, around the GG Tau (Itoh et al. 2002; McCabe et al. 2002; Krist et al. 2005; Silber et al. 2000) and UY Aur (Close et al. 1998; Hioki et al. 2007; Potter et al. 2000) binary systems. Bipolar outflows also appear in several T Tauri binary systems (e.g., Hirth et al. 1997). However, observations have focused mainly on single T

* Based on data collected at the Subaru Telescope, which is operated by the National Astronomical Observatory of Japan.

Tauri stars, although more than half of all T Tauri stars are binaries, according to observational results (separation < 1800 AU; Ghez et al. 1993; Leinert et al. 1993) and theoretical predictions (e.g., Nakamura & Li 2003; Machida et al. 2008). A limited number of studies have examined the structures around T Tauri binary systems.

FS Tauri A (hereafter FS Tau or FS Tau binary) is a classical T Tauri binary system in the Taurus molecular cloud ($d \sim 140$ pc; Elias 1978). The primary and secondary stars have spectral types of M0 and M3.5, respectively, with a projected separation, a_{sep} , of $0.242''$ (34 AU; Hartigan & Kenyon 2003). The dynamical mass of the binary is calculated to be $0.78 \pm 0.25 M_{\odot}$ (Tamazian et al. 2002). Based on the shape of the spectral energy distribution (SED), the binary is classified between Class I and II (Andrews & Williams 2005).

Gledhill & Scarrott (1989) suggested a circumbinary disk with a diameter of $\sim 5''$ (700 AU). The disk shows a linear polarization of $\sim 10\%$ in the R -band, which is higher than that of its associated molecular cloud ($\sim 2\%$; Vrba et al. 1985). However, Krist et al. (1998) could not confirm a disk beyond 60 AU from the binary using *HST* / Wide Field Planetary Camera 2 (WFPC2) observations at the V -, R -, and I -band wavelengths, although they did not subtract the point-spread functions (PSFs) of the binary. The sub-millimeter and millimeter continuum fluxes of the binary are extremely low in comparison with those of other T Tauri stars (Andrews & Williams 2005; Beckwith et al. 1990; Dutrey et al. 1996). The gas and dust mass around the binary is calculated to be $0.002 M_{\odot}$.

FS Tau is actually a hierarchical triple system. The third component, called as FS Tau B or Haro 6-5 B, is located about $20''$ (2800 AU) west of the FS Tau binary. However, high spatial resolution imaging observations revealed no directly visible star in the Haro 6-5 B system (Krist et al. 1998). Haro 6-5 B itself is obscured by its circumstellar disk, which is detected in millimeter wavelengths (Dutrey et al. 1996). The companionship of Haro 6-5 B to FS Tau A is not proven by common proper motion, spectroscopy, nor photometry. Instead, the companionship is indicated by polarimetry. The FS Tau A binary is surrounded by a reflection nebula up to 1400 AU in radius, which shows a centro-symmetric polarization pattern centered on the binary, particularly on the south side (Gledhill & Scarrott 1989). Krist et al. (1998) suggested that the north side is illuminated not only by the FS Tau binary but also by Haro 6-5 B. H_{α} imaging observations indicated a cavity wall in the north side, excited by the blue-shifted outflow from Haro 6-5 B (Eislöffel & Mundt 1998). The reflection nebula and the cavity wall appear to be truncated by the straight edge of a dark cloud ~ 700 AU north of the binary (Fig. 2; see also Fig. 3 of Krist et al. 1998).

The FS Tau binary has not been known to drive outflows. Optical emission lines, such as [S II] and H_{α} , showed no evidence of high-velocity jets from the binary (Woitas et al. 2002). Although ^{13}CO emission was observed along the southeast direction from the binary, it is unclear whether this emission arises from a diffuse wind (Dutrey et al. 1996).

In this paper, we present a subarcsecond NIR image of the FS Tau binary taken with the

Coronagraphic Imager with Adaptive Optics (CIAO) on the Subaru Telescope. Combined with the *HST* optical imaging and polarimetric methods, we discovered complex features associated with the binary. Our goal was to dissect the circumbinary disk, whose southeast side is bright in NIR wavelengths, in contrast with the northwest side, which is bright in the optical. We interpret the difference in brightness as being caused by the forward scattering of dust on the southeast side and a contribution to the radiation from Haro 6-5 B on the northwest side. Observations and data reduction are described in §2. Our results and some discussion are presented in §3 and §4, respectively. Finally, our conclusions are presented in §5.

2. Observations and Data Reduction

2.1. CIAO

Near-infrared (*H*-band; $1.6 \mu\text{m}$) coronagraphic observations of the FS Tau binary were carried out on 2007 December 17 with the Subaru/CIAO (Tamura et al. 2000) system. A $0''.8$ mask blocked the light from both the primary and secondary stars ($a_{\text{sep}} \sim 0''.24$). This mask had $\sim 2\%$ transmission (Murakawa et al. 2003). A pupil Lyot stop reduced the diffracted light. The field of view was $21''.83 \times 21''.83$, with a pixel scale of $0''.02132 \pm 0''.00003 \text{ pixel}^{-1}$ and a position angle (P.A.) on the detector of $1^\circ 58 \pm 0^\circ 07$. The pixel scale and orientation were measured with observations of the Trapezium cluster (Simon et al. 1999). One may doubt whether the astrometrical calibration is still valid, since the data of Simon et al. (1999) were taken in 1996. The pixel scale and the P.A. derived here are consistent with those derived by Itoh et al. (2005), whose data were taken in 2003. Thus we believe that these parameters are correctly derived. During the observations, the natural seeing size varied between $0''.9$ and $1''.4$ in the *H*-band. The average full width at half-maximum (FWHM) of the PSFs of our observations was $0''.4$, using AO. We obtained 36 object frames in the *H*-band. The integration time was $10 \text{ s} \times 3$ co-adds for each object frame. After obtaining the first 24 frames, we performed dithering to remove hot and bad pixels. We did not obtain science – sky – science jittering as it is the standard for infrared observations of extended sources. This is due to very low observing efficiency. For the coronagraphic observations with the AO system, the setup procedures are very complicated, as about 10 minutes was required for every pointing. After the FS Tau observations, we also obtained 25 frames of a PSF reference star, SAO 76648, in the *H*-band using the $0''.8$ mask. It is located about $140'$ east to FS Tau. The *H*-band magnitude of the PSF reference star was only 0.5 mag brighter than that of FS Tau. On the other hand, the *R*-band magnitude for the wavefront sensing is 1.5 mag brighter than that of FS Tau. We adjusted it to match FS Tau using neutral density (ND) filters in the AO. This was necessary to make the PSF of the reference star similar to that of FS Tau. The integration time was $10 \text{ s} \times 3$ co-adds for each reference star frame. FS 123 was observed as a photometric calibrator (Hawarden et al. 2001). Twilight-flats and dark frames were taken at the end of the night.

The object frames were calibrated using the Image Reduction and Analysis Facility (IRAF). First, a dark frame was subtracted from the object frames. Then the frames were divided by the normalized twilight-flat to remove pixel-to-pixel variation in sensitivity. Hot and bad pixels were removed from the divided frames using the COSMICRAYS task. Then, an averaged count in the sky region was subtracted. We judged that neither halo of the PSF nor circumstellar structures extended at $6''$ away from the central star. The count was measured along a concentric circle (radius of $\sim 6''$ with a width of $\sim 1''$) on the FS Tau binary, avoiding the diffraction artifacts of the spider. The same reduction procedures were applied to the reference star frames.

We subtracted the reference star frames from the object frames to detect faint structures buried in the halo of the central binary. The peak positions of the FS Tau binary and reference star were measured with the IMEXAMINE task on all frames. For FS Tau, the peak positions were able to be measured for 21 frames. For the rest frames, we did not identify the core of the PSF. The secondary star (FS Tau Ab) was not resolved in the object frames because the averaged FWHM was about $0''.4$. We assumed that the measured positions of the PSF peak corresponded to the positions of the primary. The object frames were shifted so that the positions of the primary were centered on the image. The reference star frames were duplicated after dark-subtraction, flat-fielding, hot and bad pixel rejection, and sky-subtraction. Then each reference star frame was shifted to adjust the peak positions of the PSFs between the reference star and each component of the binary. We calculated the positions of the secondary from the separation and P.A. in the *HST*/ACS image (see §3.2). As the binary has only a separation of $0''.23$ (32 AU) and its total mass is $0.78 M_{\odot}$ this yields an orbital period of about 210 years. Hence, the position angle of the binary could have changed up to 5° within the epoch difference of 3 years between the ACS and CIAO observations. It produces 1 pixel uncertainty ($0''.23 \times \tan 5^{\circ}$) in the position of the secondary star. The intensities of the reference star frame were scaled to adjust the flux ratio of the binary. Because the *H*-band flux ratio of the binary is unknown, we presumed that it was the same as the *K*-band flux ratio (7.0 ± 0.1 ; White & Ghez 2001). One may consider that the *H*-band flux ratio can be calculated from the spectral types of Aa and Ab and the *K*-band flux ratio. However, since FS Tau has near-infrared excess ($J = 10.705 \pm 0.027$ mag, $H = 9.244 \pm 0.026$ mag, $K = 8.178 \pm 0.017$ mag from 2MASS) and we cannot identify whether the excess arises from FS Tau Aa and/or Ab, we did not determine the flux ratio of Aa and Ab in the *H*-band. We are convinced from the final PSF-subtracted image that the assumed flux ratio is appropriate. Then the 12 reference star frames, except the frames with the asymmetric PSFs, were combined. The combined reference star frames were renormalized to match the intensities between the reference star frames and the object frames in the $0''.5 \times 0''.5$ region immediately outside the mask southwest of the binary, where the effect of the spider was negligible. The reference star frames were subtracted from each object frame. Finally, the 21 PSF-subtracted object frames, except the frames. We checked

the photometric accuracy under the unstable seeing condition. Any object except for FS Tau itself did not appear in the object frames. FS Tau in the object frames is not appropriate for evaluating the photometric accuracy, because the core of the PSF was under the mask. Instead, we evaluated it with the R -band flux of FS Tau, which was monitored during the integrations by the wavefront sensor in the AO system. The measured fluxes were stable with its standard deviation of 0.04 mag. We consider that our observations have photometric accuracy of 0.04 mag.

2.2. *HST* Polarimetric Data

Polarimetric observations were carried out on 2004 August 21 with the *HST* Advanced Camera for Surveys (ACS). These observations were proposed by D. Hines (*HST* program GO 10178). The central wavelength and the width of the F606W filter (broad V -band) are 5907 Å and 2342 Å, respectively. The field of view was $202'' \times 202''$, with a pixel scale of $0.''050 \pm 0.''005 \text{ pixel}^{-1}$ (The ACS manual). The position angles of the images were recorded in the FITS keyword of the image, ORIENTAT. The uncertainty in the position angle was $0^\circ 01 - 0^\circ 03$ in the worst cases (Koekemoer et al. 2007). The exposure time of each polarized image (0° , 60° , and 120°) was 536 s. The averaged FWHM of the observations was $0.''09$.

We downloaded the polarimetric data with the basic calibration from the *HST* MAST web site. Each frame was shifted so that the positions of the unsaturated FS Tau primary were centered on the image. The Stokes parameters, I , Q , and U were computed using

$$I = \frac{2}{3}(F_0 + F_{60} + F_{120}) \quad (1)$$

$$Q = \frac{2}{3}(2F_0 - F_{60} - F_{120}) \quad (2)$$

$$U = \frac{2}{\sqrt{3}}(F_{60} - F_{120}), \quad (3)$$

where F_0 , F_{60} , and F_{120} are the counts of each polarized image (Biretta et al. 2004). The degree of linear polarization P and the polarization angle θ were computed from

$$P = \frac{\sqrt{Q^2 + U^2}}{I} \quad (4)$$

$$\theta = \frac{1}{2} \arctan\left(\frac{U}{Q}\right). \quad (5)$$

The uncertainty in the degree of polarization was $\sim 0.3\%$, and the uncertainty in polarization angle was $< 2^\circ 0$.

We subtracted the PSFs of the primary and secondary stars in the Stokes I image from those created by the Tiny Tim program (model PSFs; Krist 2004) to detect circumbinary structures using the same data reduction as CIAO. The intensities of the model PSFs were scaled to adjust the V -band flux ratio of the binary (20.8; Krist et al. 1998). We combined the model PSF frames, and then the combined frame was renormalized to match the intensities

between the model PSF frames and the object frames of the $0''.5 \times 0''.5$ southwest region of the binary, immediately outside the "artifact region" (see §3.2).

3. Results

3.1. *H-band Coronagraphic Image*

The *H*-band coronagraphic image is shown in Fig. 1. Despite bad seeing conditions an image with $0''.4$ FWHM could be obtained. The FS Tau binary exhibited four remarkable structures:

1. A bright portion extending 630 AU southeast from the binary ("1" in Fig. 1).
2. Two arm-like structures on the western side ("2" in Fig. 1).
3. Two cavities at the northeast and southwest at P.A. $\sim 20^\circ$ and $\sim 250^\circ$, respectively ("3" in Fig. 1).
4. A faint (>17.3 mag arcsec $^{-2}$) arc-like structure ~ 900 AU west of the binary ("4" in Fig. 1).

We measured the surface brightness of the extended features with $0''.2 \times 0''.2$ square apertures. The southeast bright structure has 15.2 ± 0.3 mag arcsec $^{-2}$ at 220 AU from the central star and 16.8 ± 0.2 mag arcsec $^{-2}$ at 530 AU. If the PSF subtraction of the reference star were too strong or too weak, the residual would be seen as a circle or streak. We confirmed that the detected structures are real by making a pseudo-binary frame from the first half of the reference star frames. The projected separation and flux ratio of the pseudobinary were the same as those of the FS Tau binary (§2.1). We subtracted the PSFs using the same procedure as for FS Tau. In the processed image, we identified subtraction residuals within $1''.3 - 1''.7$ from the central star (Fig. 1). We called this region the "artifact region." Beyond this region, the diffraction pattern of the spider was the only artifact. We determined the limiting magnitude of the observations by measuring standard deviation of the sky regions which was set far from the central star and the nebulosity. We found that the limiting magnitude with S/N=3 was 17.3 mag arcsec $^{-2}$.

3.2. *F606W-band Stokes I Image*

Figure 2 represents the F606W-band Stokes *I* images of the FS Tau/Haro 6-5 B field and the closeup FS Tau binary. The primary and secondary stars of the FS Tau binary were resolved in these images. The projected separation and P.A. were $0''.23 \pm 0''.01$ and 104.69 ± 6.0 , respectively. The F606W-band image reveals the western arms ("a" in Fig. 2), the northeast and southwest cavities ("b" in Fig. 2), and the arc-like structure ("c" in Fig. 2) in common with the *H*-band coronagraphic image. Also, we discovered two eastern arms ("d" in Fig. 2) in the F606W-band image. One is sharp, but the other is not. These western and eastern arms cover the southwest and northeast cavities with opening angles of $\sim 45^\circ$ and $\sim 40^\circ$, respectively.

A local peak was identified at $1''.0$ (140 AU) from the binary in the F606W-band images before and after the PSF-subtraction ("e" in Fig. 2). The FWHM was $\sim 0''.8$ (110 AU). We identified the local peak as an extended dusty structure, not a stellar object (§4.2.2). Its F606W-band magnitude was measured to be 16.0 ± 0.5 mag arcsec $^{-2}$ with a $0''.4$ radius aperture; however, it is located in the artifact region and on the diffraction pattern of the spider.

To evaluate the PSF-subtraction in the *HST* image, a pseudo-PSF binary was created using a dwarf, 2MASS J07040548-0350493 (*HST* program GO 9588 proposed by H. Bond). The flux ratio of the pseudo-binary was set to that of the FS Tau binary (20.8; Krist et al. 1998). The projected separation of the pseudo-binary had the same value as the FS Tau binary in the F606W-band image. We subtracted the PSFs created by the Tiny Tim from the pseudo-binary. The PSF-subtraction produced artifacts within about $1''.6$ from the central star (Fig. 2). The limiting magnitude of the observations was calculated from standard deviation of the sky regions, which was set far from the central star and the nebulosity. We derived that the limiting magnitude with S/N=3 was 22.1 mag arcsec $^{-2}$.

3.3. F606W-band Polarimetric Image

Figure 3 represents the F606W-band polarized intensity image and *H*-band coronagraphic image, together with polarization vectors. To clarify the sources of the polarizations around the FS Tau binary, the polarization angles were investigated. We defined the deviation from the centro-symmetric polarization angle centered on the binary and Haro 6-5 B as $\theta_{\text{centroA}} = |\theta - \text{P.A.}_{\text{A}\perp}|$, and $\theta_{\text{centroB}} = |\theta - \text{P.A.}_{\text{B}\perp}|$. These angles represent the observed polarization angles; $\text{P.A.}_{\text{A}\perp}$ and $\text{P.A.}_{\text{B}\perp}$ are perpendicular to the P.A. with respect to the FS Tau primary and Haro 6-5 B, respectively, at each position. The red-painted polarization vectors in Figure 3 represent $\theta_{\text{centroA}} < 30^\circ$ and $\theta_{\text{centroB}} > 30^\circ$; the blue-painted polarization vectors $\theta_{\text{centroA}} < 30^\circ$ and $\theta_{\text{centroB}} < 30^\circ$; the green-painted polarization vectors $\theta_{\text{centroA}} > 30^\circ$ and $\theta_{\text{centroB}} < 30^\circ$; the yellow-painted polarization vectors $\theta_{\text{centroA}} > 30^\circ$ and $\theta_{\text{centroB}} > 30^\circ$. If the FS Tau binary were the only illuminating source in the FS Tau/Haro 6-5 B field, the angles θ_{centroA} would fall below 30° at all points. This means that the blue-painted polarization vectors would be present between the P.A. = 57° to 135° and 250° to 303° if the binary had a geometrically flat circumbinary disk with a major axis along a P.A. = 30° and an inclination by 35° (§4.1.1). The red-painted polarization vectors would be present at the other P.A.s. Their degrees of polarization depend on the scattering angles.

The FS Tau binary system has two polarimetric characteristics: small θ_{centroA} features at the local peak ($\theta_{\text{centroA}} = 5^\circ \pm 4^\circ$), the southwest arm ($7^\circ \pm 5^\circ$), and the western cavity ($13^\circ \pm 11^\circ$); and large θ_{centroA} features at the portion of the southeast that is bright in the *H*-band ($30^\circ \pm 22^\circ$) and at the north side at a distance from the binary, r , of $r > 420$ AU ($53^\circ \pm 17^\circ$). Causes of these large deviations in the polarization angles will be discussed in the next section. The polarized image does not show parallel polarization vectors or null points near

the central binary both of which are indicative of a polarization disk. The averaged F606W-band polarization was $P = 11 \pm 5\%$ in $r < 560$ AU, which is consistent with the result of Gledhill & Scarrott (10% at the R -band).

4. Discussion

4.1. Circumbinary Disk

We consider that the emission nebulae are mostly attributed to the circumbinary disk.

4.1.1. Optical and NIR Imaging/Polarimetric Characteristics of the Disk

Figure 4 shows the H -band radial profile along the bright southeast region. The H -band brightness was 15.2 ± 0.3 mag arcsec $^{-2}$ at $r = 220$ AU and 16.8 ± 0.2 mag arcsec $^{-2}$ at $r = 530$ AU. We fit a single power-law of $r^{-1.9 \pm 0.1}$ to the southeast region. Its slope was shallower than that of circumstellar disks around other classical T Tauri stars, such as FN Tau (-2.5; Kudo et al. 2008), TW Hya (-2.6; Weinberger et al. 2002), and GM Aur (-3.5; Schneider et al. 2003), in the H -band. The surface brightness of a geometrically flat and optically thick structure fits a single power-law of r^{-3} , whereas the surface brightness of a flared structure with well-mixed gas and dust fits a power law of r^{-2} (Whitney & Hartmann 1992). We argue that the southeast region corresponds to a part of the circumbinary disk and is more flared than the other T Tauri disks. One may consider that the structure is a flattened envelope rather than a disk. But the central binary is not heavily reddened. The combined near-infrared colors are $J - H = 1.46 \pm 0.04$ mag and $H - K = 1.07 \pm 0.03$ mag, corresponding to the intrinsic colors of classical T Tauri stars (Meyer et al. 1997) with a moderate extinction ($A_V \sim 6$ mag). Based on these colors, we consider that the structure is a circumbinary disk. The H -band radial profile of the northwest region of the binary are also shown in Figure 4. It is fainter than the southeast region at all distances. We fit a single power-law of $r^{-1.5 \pm 0.3}$ to the northwest region. Its slope seems shallower than that of the southeast region, but its faintness prevents us from further discussion.

Figure 5 represents the F606W-band azimuthal profiles of the degrees of polarization around the FS Tau binary. The degrees of polarization were derived from a $0''.25 \times 0''.25$ aperture. We determined that the outer radius of the disk is consistent with that of the southeast region ($4''.5 = 630$ AU), which is bright in the H -band. The observed polarizations of $\theta_{\text{centroA}} > 30^\circ$ (i.e., the green- and yellow-painted vectors in Fig. 3) were not applied in order to exclude the polarizations caused by multiple scattering events from dust grains in the southeast region (§4.1.4). In addition, the polarizations in the $r > 3''$ north (P.A. = 280° to 55°) were masked due to the contamination by light from the cavity wall associated with Haro 6-5 B (§4.1.2). The maximum degrees of polarization, P_{max} , were observed in the northeast and southwest sides of the disk, and the minima, P_{min} , were observed in the southeast and northwest sides.

We constructed a simple circumbinary disk model to investigate the polarization by dust grains in the FS Tau binary system. The FS Tau binary has a prominent smooth emission feature at $10\ \mu\text{m}$ (Furlan et al. 2006), which indicates sub-micron-sized amorphous silicate dusts in the disk surface layer. Such dust grains show Rayleigh-like scattering. The GG Tau binary also shows a strong $10\ \mu\text{m}$ silicate emission feature similar to that of the FS Tau binary (Furlan et al. 2006). The circumbinary disk around GG Tau displays a high polarization amplitude ($\sim 50\%$), with a centro-symmetric pattern in the NIR wavelengths (Silber et al. 2000), which is well reproduced by Rayleigh-like scattering ($a \ll \lambda$) from sub-micron dust grains in the disk. Therefore, we assume that "single" Rayleigh-like scattering occurs in the FS Tau circumbinary disk. Using small dust grains with a power-law size distribution of $n(a) \propto a^{-3.5}$ between $0.005 - 0.25\ \mu\text{m}$ (hereafter MRN dust; Mathis et al. 1977), the degree of polarization, P , depends on the scattering angle, θ_{scat} , as below:

$$P = \frac{I_{\perp} - I_{\parallel}}{I_{\perp} + I_{\parallel}} = \frac{1 - \cos^2 \theta_{\text{scat}}}{1 + \cos^2 \theta_{\text{scat}}}; \quad (6)$$

$$\theta_{\text{scat}} = \cos^{-1} \left(\frac{y \tan(i \pm \phi)}{(x^2 + y^2 + y \tan(i \pm \phi))^2} \right), \quad (7)$$

where I_{\parallel} and I_{\perp} are the intensities of scattered light in polarization modes parallel and perpendicular to the scattering plane, respectively (van de Hulst 1957). The symbol i is the disk inclination, ϕ is the flared angle of the disk, and x , y are the coordinates deprojected along the major and minor disk axes, respectively, with their origin at the center of the primary star (Fig. 5), i.e., $+\phi$ for the near side of the disk along our line of sight and $-\phi$ for the far side. Three parameters, i , ϕ , and the P.A. of the disk major axis, ξ , are free parameters. These parameters were determined from a χ^2 minimization method at $r = 1''$ intervals.

The disk model shows a centro-symmetric polarization pattern around the binary. The P_{max} occurs at two points, each at a 90° scattering angle (i.e., disk major axis). The disk minor axis corresponds to the positions of the P_{min} , where the scattering angles are far from 90° . If the disk is flared, P_{min} occurs at the near side of the disk. Notice that a spherical dust distribution, such an envelope, does not produce a sinusoidal pattern; in that case, the degree of polarization is constant as a function of the scattering angle (or P.A.). Because the observed P_{max} occurs at P.A. = 30° and 210° at $r = 2 - 3''$ (280 – 420 AU; Fig. 5 and Table 1), we determined the disk major axis at P.A. = 30° and a disk inclination of 35° . The flat disk model ($\phi = 0^\circ$) agree well with the observed polarization at $r = 2 - 3''$. The polarization is at a minimum at P.A. = 120° and 300° . Assuming the southeast side is brighter than the northwest side in the H -band due to the forward scattering of dust, the southeast side is located closer to us ($\theta_{\text{scat}} \sim 55^\circ$), and the northwest side is oriented away from us ($\theta_{\text{scat}} \sim 125^\circ$). However, the radial profile of the surface brightness of the disk is not consistent with the flat-disk model. The χ^2 minimization method shows that the southeast side of the disk has a lower degree of polarization than the northwest side at $r = 4 - 4.5''$ (560 – 630 AU). The flared disk model

($\phi = 5^\circ$) possibly explains the observed polarization at $r = 4 - 4.5''$, where the disk is inclined by 30° , with its southeast side toward us.

The P.A. of the disk major axis and the inclination of the disk are consistent with those of the binary orbit, whose major axis is along the P.A. = $18^\circ \pm 7^\circ$ and an inclination of $20^\circ \pm 5^\circ$ (Tamazian et al. 2002). The χ^2 minimization method also shows $(\xi, i, \phi) = (15^\circ, 40^\circ, 0^\circ)$ at $1 - 2''$ and $(35^\circ \text{ to } 40^\circ, 30^\circ \text{ to } 35^\circ, 0^\circ \text{ to } 5^\circ)$ at $3 - 4''$.

In conclusion, the circumbinary disk is characterized by the following geometry: the radius of the disk is 630 AU ($4''.5$), the disk major axis is along the P.A. = 15° to 40° , and the disk is inclined by 30° to 40° , where the southeast side (P.A. = 105° to 130°) corresponds to the side nearest to us. The outer (>560 AU) portion of the disk is possibly more flared than its inner portion.

4.1.2. Southeast to Northwest Brightness Asymmetry

The circumbinary disk shows an unambiguous southeast-northwest asymmetry. The brightness ratio of the southeast and northwest sides at $r = 280 - 630$ AU is 1.6 ± 0.4 in the H -band. We suggest that anisotropic scattering of the dust causes the asymmetric brightness of the disk and that the southeast side is brighter due to forward scattering of the dust. This indicates that the southeast side corresponds to the near side. Based on this hypothesis, the brightness ratio ($B_{\text{near}}/B_{\text{far}}$) of the disk is described as:

$$\frac{B_{\text{near}}}{B_{\text{far}}} = \left(\frac{1 + g^2 - 2g \cos \bar{\theta}_{\text{Nscat}}}{1 + g^2 - 2g \cos \bar{\theta}_{\text{Fscat}}} \right)^{-3/2}, \quad (8)$$

where g is the asymmetry parameter of the Henyey-Greenstein scattering phase function (Henyey & Greenstein 1941), $\bar{\theta}_{\text{Nscat}}$ is the averaged scattering angle of the near side, and $\bar{\theta}_{\text{Fscat}}$ is that of the far side (Eq. 7). For the disk parameters in §4.1.1 ($r = 630$ AU, $\xi = 15^\circ$ to 40° , $i = 30^\circ$ to 40° , and $\phi = 0^\circ$ to 5°), the H -band brightness ratio was fit with $g \sim 0.2$. This value is consistent with that of the MRN dust ($g \sim 0.1$) shown by Kim et al. (1994), who assumed single scattering by the dust in a diffuse interstellar cloud ($R_V = 3.1$). For the FS Tau circumbinary disk, such small dust grains probably produce single-scattered light, as the disk is optically thin in the H -band (§4.1.4).

4.1.3. Northwest Side of the Binary

The northwest side of the circumbinary disk are bright in the optical wavelengths but faint in the near-infrared wavelengths (Fig. 6). We measured its color. Within $1''.5$ from the central star, the PSF subtractions are not perfect either in the optical image nor in the near-infrared image. Beyond $4''$ from the central star the disk is very faint in the near-infrared wavelengths. We measured the surface brightness of the disk in the region between $1''.5$ and $4''.0$ from the central star and the P.A. between 280° and 355° . The F606W– H color in this region was derived to be between 1.7 mag and 3.0 mag. We also derived the intrinsic colors, $(F606W-H)_{\text{int}}$, of the photosphere of the binary and Haro 6-5 B as 2.44 ± 0.02

mag and 2.00 ± 0.02 mag, respectively, using the relationship $(F606W-H)_{\text{int}} = (V-H)_{\text{int}} - (0.477 \pm 0.013)(V-R)_{\text{int}} + (0.001 \pm 0.005)(V-R)_{\text{int}}^2$ (Sirianni et al. 2005). The intrinsic colors, $(V-R)_{\text{int}}$ and $(V-H)_{\text{int}}$, were derived from those of main sequence stars (Ducati et al. 2001) whose spectral types were the same as the FS Tau primary (M0; Hartigan & Kenyon 2003) and Haro 6-5 B (K5; White & Hillenbrand 2004). Comparing the disk color with the colors of the point sources, we cannot identify whether the disk is illuminated by the FS Tau binary or Haro 6-5 B.

On the other hand, the polarization map clearly indicates the contribution of Haro 6-5 B. We claim that the scattered light and optical emission lines from Haro 6-5 B change the degree of polarization and polarization angle on the north side at $r > 3''$. Several observations identified a cavity wall in the north side, which is created by the blue-shifted outflow from Haro 6-5 B (Gledhill & Scarrott 1989; Eislöffel & Mundt 1998). Gledhill & Scarrott (1989) reported that the cavity wall has non-centro-symmetric polarization patterns with respect to the FS Tau binary, bluer colors than those of the south side of the binary, and an H_α emission line. We confirm the radiation from Haro 6-5 B at $r > 3''$ north (P.A. = 280° to 55°) in the F606W-band polarimetric image. The green-painted polarization vectors are predominant (56% of the total) in the $r > 3''$ north side (Fig. 3). The averaged θ_{centroA} is $53^\circ \pm 17^\circ$, whereas the averaged θ_{centroB} is $11^\circ \pm 8^\circ$. The averaged P is $16 \pm 7\%$. These θ_{centroB} and P are comparable to those of the cone-shaped reflection nebula (hereafter R1 nebula) that extends $8''$ northeast from its illuminating source Haro 6-5 B. In addition, the radiation from Haro 6-5 B is a possible cause of the blue-painted polarization vectors at $r > 3''$ north. The averaged θ_{centroA} is slightly larger than the averaged θ_{centroB} ($20^\circ \pm 7^\circ$ vs. $14^\circ \pm 9^\circ$). We argue that the cavity wall blocks the north side of the circumbinary disk at $r > 3''$. On the other hand, for the north side at $r < 3''$, the averaged θ_{centroA} is $13^\circ \pm 13^\circ$ and the averaged θ_{centroB} is $44^\circ \pm 24^\circ$, indicating the scattered light from the FS Tau binary.

4.1.4. Southeast Side of the Disk

The southeast side of the circumbinary disk is bright in the near-infrared wavelengths but faint in the optical wavelengths (Fig. 6). We measured its color in the region between $1''.5$ and $4''.5$ from the central star and the P.A. between 93° and 175° . The F606W– H color of this region of the disk is derived to be 4.2 ± 0.2 mag, which is redder than the intrinsic color of the FS Tau binary (Fig. 6). Figure 3 displays a weak centro-symmetric ($\theta_{\text{centro}} \sim 30^\circ$) polarization pattern around the southeast portion, despite the high signal to noise ratio (≥ 6). We consider that the southeast portion corresponds to a part of the circumbinary disk.

Given the $(F606W-H)_{\text{int}}$ of the binary (2.44 ± 0.02 mag) and the F606W– H color of the southeast portion (4.2 ± 0.2 mag), the color excess of the southeast portion is $E(F606W-H) = 1.8 \pm 0.2$ mag. We assume that extinction by dust grains around the binary reddens the southeast portion. This extinction, A_λ , was derived as 2.3 ± 0.3 mag in the F606W-band and 0.5 ± 0.1 mag at the H -band. We estimated an optical depth, τ_λ , of 2.1 ± 0.3 in the F606W-band and

0.5 ± 0.1 at the H -band, using the relationship $A_\lambda = 1.086\tau_\lambda$ (e.g., Stark et al. 2006). Thus, the southeast portion is optically thick in the F606W-band, and some of the scattered light comes from the southeast portion, where it expected multiple scattering events from dust grains. Further circular polarization observations are needed to perceive the multiple scattered light events.

4.2. Outflow

No optical jet was detected within a few arcseconds of the FS Tau binary (Woitas et al. 2002). Although ^{13}CO emission was observed along the southeast side, it is unknown whether this emission arises from the diffuse wind from the binary (Dutrey et al. 1996). The circumbinary disk model (§4.1.1) predicts a red-shifted outflow driven by the primary or secondary stars along the southeast direction (P.A. = 105° to 135°), given that the circumstellar disks are coplanar with the circumbinary disk, and the outflow axis is perpendicular to the circumstellar disk plane.

In contrast, both the H -band and F606W-band images show evidence of other outflows: the western and eastern arms + cavity systems, and the arc-like structure (Figures 1 and 2). The arc-like structure located at $r \sim 900$ AU west is seen faintly in the H -band image, but is clearly detected at above 10σ in the F606W-band image. This structure appears to connect the western arms or to have an appearance similar to bow shocks excited by Herbig-Haro flows. The two western arms encompass the southwest cavity with an opening angle of $\sim 45^\circ$. The eastern arms + cavity system, only detected in the F606W-band image, plausibly mixes with the cavity wall associated with Haro 6-5 B (§4.1.3). We argue that these arms + cavity systems are similar to the features created by bipolar outflows in several T Tauri systems (e.g., Haro 6-5 B: Eislöffel & Mundt 1998, HL Tau; Lucas et al. 2004). We measured surface brightness of the cavities. The regions of the cavities were defined as circular areas with $3''.5$ radius centered at $12''.4$ with the P.A. of $43^\circ.5$ from the central star and centered at $9''.9$ with P.A.= $245^\circ.7$ for the northeast cavity and the southwest cavity, respectively. The (b) marks of the right figure of Fig. 2 correspond to the central positions of the cavity regions. The southwest and northeast cavities have comparable F606W-band brightnesses of 21.2 ± 0.2 mag arcsec $^{-2}$, whereas their H -band brightness are lower than the limiting magnitude (17.3 mag arcsec $^{-2}$). Their F606W– H colors are < 3.9 mag i.e., $\tau_{\text{F606W}} < 1.9$ and $\tau_{\text{H}} < 0.4$ (see §4.1.4), assuming that the cavities are reddened by dust extinction. The outflow from the binary would sweep up materials in the cavities. The polarization of the northeast cavity is $18 \pm 5\%$, and that of the southwest cavity is $19 \pm 6\%$. These polarizations are relatively higher than the other structures located within 560 AU of the binary (11%). The southwest cavity shows $\theta_{\text{centroA}} = 13^\circ \pm 11^\circ$, indicating the efficiently scattered light from the binary. The northeast cavity has $\theta_{\text{centroA}} = 22^\circ \pm 15^\circ$ and $\theta_{\text{centroB}} = 22^\circ \pm 10^\circ$. The northeast cavity is illuminated by mixed radiation from the binary and Haro 6-5 B, although the dereddened color of the mixed radiation is unclear. We claim

that the outflow emanates to the P.A. = 220° to 250° , which is equal to the axisymmetric orientation of the western arms. This direction is not consistent with that calculated by our disk model (P.A. = 105° to 135° or 285° to 315°). These differences are possibly produced by the mechanisms discussed in the following sections.

4.2.1. *Disk Misalignment*

One possible mechanism is that the primary/secondary circumstellar disks are not coplanar with the circumbinary disk. For T Tauri binaries separated by several AU (e.g., DQ Tau; Mathieu et al. 1997, UZ Tau E; Prato et al. 2002) and T Tauri binaries with moderate separation (e.g., GG Tau; Tamazian et al. 2002), the circumbinary disks are coplanar with each binary orbital plane. In contrast, for widely separated T Tauri binary systems, *K*-band polarimetric observations suggest that circumstellar disks are not perfectly coplanar but differ slightly from each other ($\sim 20^\circ$; Jensen et al. 2004).

Bate et al. (2000) demonstrated that during about 2000 binary orbital periods circumstellar disks are roughly aligned with a binary orbital plane by tidal torques. This timescale is estimated to be 5.5×10^5 yrs for the FS Tau binary, given its separation of 39 AU and its total binary mass of $0.78 M_\odot$ (Tamazian et al. 2002). We suggest, based on a comparison of the alignment timescale with the stellar age based on the shape of the SED ($10^5 - 10^6$ yrs; Andrews & Williams 2005), that the circumbinary disk is still misaligned with the circumstellar disks.

4.2.2. *Gravitational Instability and Inhomogeneous Distributions of the Disk Materials*

Another possibility is that the western and eastern arms are formed by other mechanisms, such as gravitational disk instability or inhomogeneous distributions of the circumbinary materials.

A circumstellar disk associated with AB Aur has spiral arms that are expected to be formed by the gravitational instability of the disk (Fukagawa et al. 2004). Nelson et al. (1998) revealed that such a spiral arm appears in a circumstellar disk if $Q \leq 2.0$, where $Q = c_s \Omega / (\pi G \Sigma)$ is Toomre's Q -value, c_s is the sound speed, Ω is the angular velocity, and Σ is the surface density of the disk. However, the FS Tau circumbinary disk is less massive ($0.002 M_\odot$; Andrews & Williams 2005). Its Toomre's Q -value is much larger than 2.0, given the disk radius of 630 AU, the surface density distribution of $\Sigma \propto r^{-0.5}$ (Kitamura et al. 2002), and $c_s = 190 \text{ m s}^{-1}$ ($T = 10$ K, for typical T Tauri disks). Thus, we conclude that gravitational disk instability does not occur in the circumbinary disk.

The second possible mechanism is that a companion shapes the spiral arm-like features (e.g., Bate et al. 2003). However, high spatial resolution observations have detected no other companion around the FS Tau binary (Chen et al. 1990; Simon et al. 1992; Krist et al. 1998; Hartigan & Kenyon 2003; Connelley et al. 2009). We identified a local peak at $r \sim 140$ AU north in the F606W-band polarimetric images ("e" in Fig. 2 and "A" in Fig 3). This structure corresponds to the "small arc" detected by Krist et al. (1998). This local peak is extended (its FWHM of 110 AU) and shows $P = 15\%$ and $\theta_{\text{centroA}} = 5^\circ$. These indicate that the local peak

is an extended dusty structure associated with the binary, not a stellar companion. The lower limit of the local peak mass is estimated to be $\sim 0.3 M_{\oplus}$ from its F606W-band brightness ($16.0 \text{ mag arcsec}^{-2}$). Such a low mass structure cannot create the disk instability.

Finally, several studies have demonstrated arm-like structures as resulting from inhomogeneous distributions of materials in a circumbinary disk (Günther & Kley 2002; Ochi et al. 2005). The observed local peak could be such an inhomogeneity. However, no inhomogeneous gas and dust structures around the binary are detected in the millimeter wavelength observations due to insufficient spatial resolution ($\sim 3''$) and flux sensitivity (Dutrey et al. 1996; Andrews & Williams 2005). The Atacama Large Millimeter/submillimeter Array (ALMA) will clarify whether the arms + cavity systems correspond to outflowing materials or to a part of the Keplerian circumbinary disk.

5. Conclusions

Using the Subaru/CIAO, we obtained an H -band coronagraphic image of the T Tauri binary system FS Tau. Combined with the HST/ACS (F606W) polarimetric images, several features around the binary were identified.

The circumbinary disk extends to 630 AU in radius. The disk is inclined by 30° to 40° , such that the southeast side is nearest. The outer portion of the disk may be more flared than the inner portion. The disk also displays an unambiguous southeast-northwest brightness asymmetry. The southeast side of the disk is significantly red ($F606W-H = 4.2 \pm 0.2 \text{ mag}$). It shows a weak centro-symmetric ($\theta_{\text{centroA}} \sim 30^\circ$) polarization pattern in the F606W-band. These indicate multiple scattering events in the optically thick southeast side at F606W-band wavelengths. The northeast side of the binary is about neutral in color ($F606W-H = 1.7 \text{ mag}$ or 3.0 mag) compared with the FS Tau binary and Haro 6-5 B. We argue that the northwest side of the binary at $r > 420 \text{ AU}$ ($3''$) is blocked by the cavity wall associated with Haro 6-5 B. This idea is supported by the observed polarization angles ($\theta_{\text{centroA}} = 53^\circ \pm 17^\circ$ and $\theta_{\text{centroB}} = 11^\circ \pm 8^\circ$). The $r < 420 \text{ AU}$ northwest side has $\theta_{\text{centroA}} = 13^\circ \pm 13^\circ$ and $\theta_{\text{centroB}} = 44^\circ \pm 24^\circ$, indicating scattered light from the FS Tau binary.

The western cavity encompassed by the two arm structures is detected in both the F606W-band and H -band images. The eastern cavity, with additional arms, is seen in the F606W-band image, but only the cavity appears in the H -band. We argue that these arms + cavity systems are created by the bipolar outflow from the binary along the P.A. = 220° to 250° . Another interpretation is that these structures correspond to inhomogeneous distributions of materials in the disk. Further high spatial and velocity resolution observations at sub-millimeter and millimeter wavelengths (e.g., ALMA) are required to clarify the mechanisms of these structures.

We thank the telescope staff members and operators at the Subaru Telescope. We are

grateful for fruitful discussions with Tadashi Mukai. The *HST* data presented in this paper were obtained from the Multimission Archive at the Space Telescope Science Institute (MAST). This study was partly supported by the Global Centers of Excellence (GCOE) Program: "Foundation of International Center for Planetary Science" from the Ministry of Education, Culture, Sport, Science, and Technology (MEXT). T. H. is financially supported by the Japan Society for the Promotion of Science (JSPS) for Young Scientists.

References

- Acke, B., Min, M., van den Ancker, M. E., Bouwman, J., Ochsendorf, B., Juhasz, A., & Waters, L. B. F. M. 2009, *A&A*, 502, L17
- Armitage, P. J., Clarke, C. J., & Tout, C. A. 1999, *MNRAS*, 304, 425
- Artymowicz, P., & Lubow, S. H. 1994, *ApJ*, 421, 651
- Artymowicz, P., & Lubow, S. H. 1996, *ApJ*, 467, L77
- Andrews, S. M. & Williams, J. P. 2005, *ApJ*, 631, 1134
- Bate, M. R., Bonnell, I. A., Clarke, C. J., Lubow, S. H., Ogilvie, G. I., Pringle, J. E., & Tout, C. A. 2000, *MNRAS*, 317, 773
- Bate, M. R., Lubow, S. H., Ogilvie, G. I., & Miller, K. A. 2003, *MNRAS*, 341, 213
- Beckwith, S. V. W., Sargent, A. I., Chini, R. S. & Guesten, R. *AJ*, 1990, 99, 924
- Biretta, J., Kozhurina-Platais, V., Boffi, F., Sparks, W., & Walsh, J. 2004, Instrument Science Report ACS 2004-09 (Baltimore: STScI)
- Boss, A. P. 2002, *ApJ*, 568, 743
- Chen, W. P., Simon, M., Longmore, A. J., Howell, R. R., & Benson, J. A. 1990, *ApJ*, 357, 224
- Close, L. M., et al. 1998, *ApJ*, 499, 883
- Connelley, M. S., Reipurth, B., & Tokunaga, A. T. 2009, *AJ*, 138, 1193
- Ducati, J. R., Bevilacqua, C. M., Rembold, S. B., & Ribeiro, D. 2001, *ApJ*, 558, 309
- Dutrey, A., Guilloteau, S., Duvert, G., Prato, L., Simon, M., Schuster, K., & Menard, F. 1996, *A&A*, 309, 493
- Eisloffel, J. & Mundt, R. 1998, *AJ*, 115, 1554
- Elias, J. H. 1978, *ApJ*, 224, 857
- Ferland, G. & Netzer, H. 1979, *ApJ*, 229, 274
- Fukagawa, M., et al. 2004, *ApJ*, 605, L53
- Ghez, A. M., Neugebauer, G., & Matthews, K. 1993, *AJ*, 106, 5
- Gledhill, T. M. & Scarrott, S. M. 1989, *MNRAS*, 236, 139
- Günther, R. & Kley, W. 2002, *A&A*, 387, 550
- Hartigan, P. & Kenyon, S. J. 2003, *ApJ*, 583, 334
- Hawarden, T. G., Leggett, S. K., Letawsky, M. B., Ballantyne, D. R., & Casali, M. M. 2001, *MNRAS*, 325, 563
- Heney, L. G. & Greenstein, J. L., 1941, *ApJ*, 93, 70
- Hioki, T., et al. 2007, *AJ*, 134, 880
- Hioki, T., et al. 2009, *PASJ*, 61, 1271

Hirth, G. A., Mundt, R., & Solf, J. 1997, *A&AS*, 126, 437
Itoh, Y., et al. 2002, *PASJ*, 54, 963
Itoh, Y., et al. 2005, *ApJ*, 620, 984
Jensen, E. L. N., Mathieu, R. D., Donar, A. X., & Dullighan, A. 2004, *ApJ*, 600, 789
Kim, S.-H., Martin, P. G., & Hendry, P. D. 1994, *ApJ*, 422, 164
Kitamura, Y., Momose, M., Yokogawa, S., Kawabe, R., Tamura, M., & Ida, S. 2002, *ApJ*, 581, 357
Koekemoer, A. M. et al. 2007, *ApJS*, 172, 196
Krist, J. E., et al. 1998, *ApJL*, 501, 841
Krist, J. E. 2004, *Tiny Tim User's Manual V 6.3*
Krist, J. E., et al. 2005, *AJ*, 130, 2778
Krist, J. E., Stapelfeldt, K. R., Hester, J. J., Healy, K., Dwyer, S. J., & Gardner, C. L. 2008, *AJ*, 136, 1980
Kudo, T., et al. 2008, *ApJ*, 673, L67
Leinert, Ch., et al. 1993, *A&A*, 278, 129
Lucas, P. W., et al. 2004, *MNRAS*, 352, 1347
Machida, M. N., Tomisaka, K., Matsumoto, T., & Inutsuka, S. 2008, *ApJ*, 677, 327
McCabe, C., Duchêne, G., & Ghez, A.M. 2002, *ApJ*, 575, 974
Mathieu, R. D., et al., 1997, *AJ*, 113, 1841
Mathis, J. S., Rumpl, W., & Nordsieck, K. H. 1977, 217, 425
Mathis, J. S. 1990, *aap*, 28, 37
Murakawa, K., et al. 2003, *Proc. SPIE*, 4841, 881
Nakamura, F. & Li, Zhi-Yun. 2002, *ApJ*, 566, 101
Nelson, A. F., Benz, W., Adams, F. C., & Arnett, D. 1998, *ApJ*, 502, 342
Ochi, Y., Sugimoto, K., & Hanawa, T. 2005, *ApJ*, 623, 922
Pety, J., Gueth, F., Guilloteau, S., & Dutrey, A. 2006, *A&A*, 458, 841
Pinte, C., Fouchet, L., Menard, F., Gonzalez, J. F., & Duchêne, G. 2007, *A&A*, 469, 963
Potter, D. E., Close, L. M., Roddier, F., Roddier, C., Graves, J. E., & Northcott, M. 2000, *ApJ*, 540, 422
Prato, L., Simon, M., Mazeh, T., Zucker, S., & McLean, I. S. 2002, *ApJ*, 579, L99
Roberge, A., Weinberger, A. J., & Malumuth, E. M. 2005, *ApJ*, 622, 1171
Schneider, G., et al. 2003, *AJ*, 125, 1467
Silber, J., Gledhill, T., Duchêne, G., & Menard, F. 2000, *ApJ*, 536, L89
Simon, M., Chen, W. P., Howell, R. R., Benson, J. A., & Slowik, D. 1992, *ApJ*, 384, 212
Simon, M., Close, L. M., & Beck, T. L. 1999, *AJ*, 117, 1375
Sirianni, M., et al. 2005, *PASP*, 117, 1049
Stapelfeldt, K. R., et al. 1998, *ApJ*, 508, 736
Stark, D. P., Whitney, B. A., Stassun, K., & Wood, K. 2006, *ApJ*, 649, 900
Takami, M., Beck, T. L., Pyo, T.-S., McGregor, P., & Davis, Ch. 2007, *ApJ*, 670, 33
Tamazian, V. S., Docobo, J. A., White, R. J., & Woitas, J. 2002, *ApJ*, 578, 925
Tamura, M., & Sato, S. 1989, *AJ*, 98, 4
Tamura, M., et al. 2000, *Proc. SPIE*, 4008, 1153

- van de Hulst, H. C. 1957, *Light Scattering by Small Particles* (New York:Wiley)
- Vrba, F. J., Rydgren, A. E., & Zak, D. S. 1985, *AJ*, 90, 2074
- Weinberger, A., et al. 2002, *ApJ*, 566, 409
- Weintraub, D. A., Goodman, A. A., & Akeson, R. L. 2000, in *Protostars and Planets IV*, ed. V. Mannings, A. P. Boss, & S. S. Russell (Tucson, AZ: Univ. Arizona Press), 247
- White, R. J., Ghez, A. M., Reid, I. N., & Schultz, G. 1999, *ApJ*, 520, 811
- White, R. J. & Ghez, A. M. 2001, *ApJ*, 556, 265
- White, R. J., & Hillenbrand, L. A. 2004, *ApJ*, 616, 998
- Whitney, B., & Hartmann, L., 1992, *ApJ*, 395, 529
- Whitney, B. A., Kenyon, S. J., & Gomez, M. 1997, *ApJ*, 485, 703
- Woitak, J., Eisloffel, J., Mundt, R. & Ray, T. P., 2002, *ApJ*, 564, 834
- Wood, K., Crosas, M., & Ghez, A. 1999, *ApJ*, 516, 335

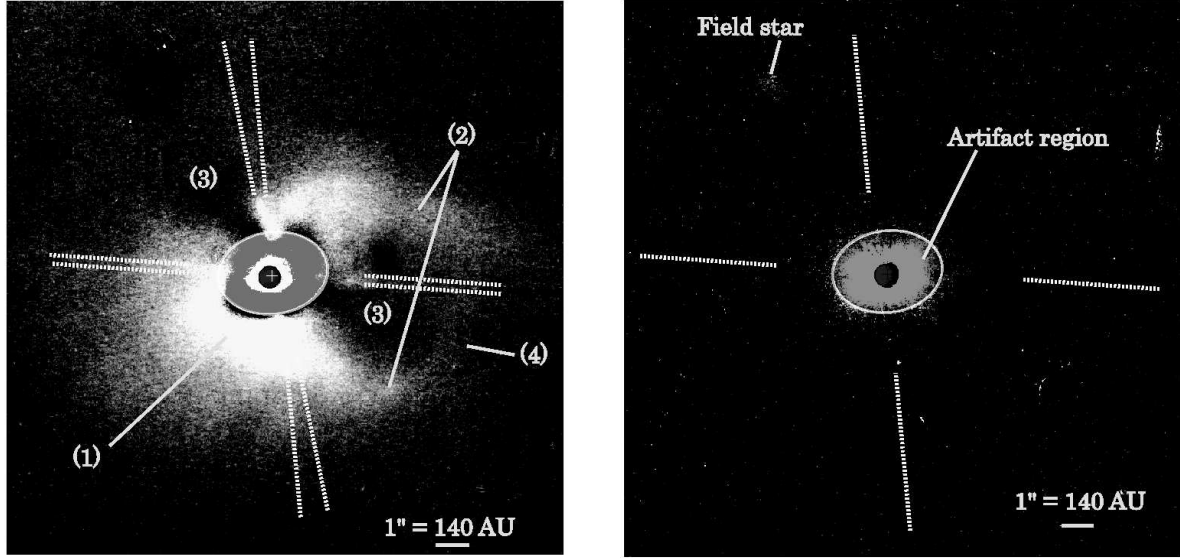


Fig. 1. The H -band coronagraphic image of the FS Tau binary system (*left*). The PSFs of the central binary were subtracted. "1" indicates the H -band bright portion of the circumbinary disk; "2" indicates the arm-like structures; "3" indicates the cavities; and "4" indicates the arc-like structure. The position of the FS Tau primary is indicated by the cross symbol in the occulting mask with a diameter of $0''.8$ (112 AU; a circular symbol). The binary is not resolved due to bad seeing conditions. The pseudo-binary was created using the PSF reference star SAO 76648 (*right*). The PSF-subtracted image shows some artifacts within $1''.3 - 1''.7$ from the central star, represented as hatched ellipses in both images. Beyond this region, the diffraction pattern of the spider is the only artifact, indicated by dotted lines in the both images. The field of view (FOV) is $17''.8 \times 17''.8$. North is up and east is to the left.

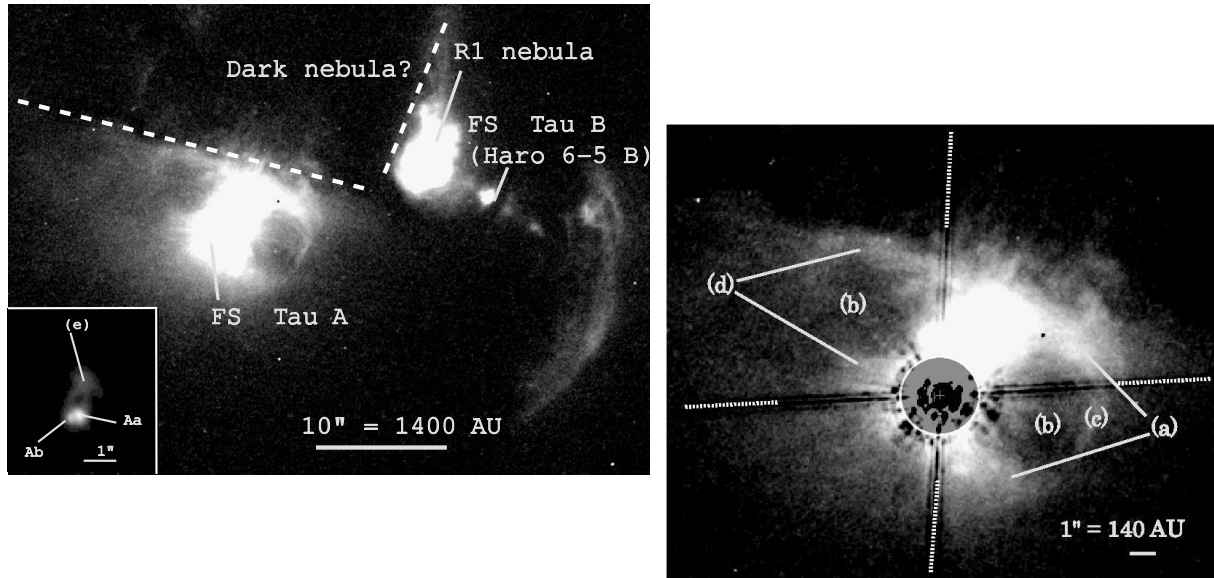


Fig. 2. The F606W-band Stokes I images of the FS Tau/Haro 6-5 B field before subtracting the PSFs of the central binary (*left*) and a closeup of the binary after subtracting the PSFs (*right*). "a" represents the western arms, "b" the cavities, "c" the arc-like structure, and "d" the eastern arms. The artifact region is shown by the hatched ellipse. The directions of the spider pattern are indicated by dotted lines. "e" represents the local peak in the logarithmic image of the FS Tau binary at lower left of the top panel. The positions of the FS Tau primary and secondary stars are indicated by the big and small cross symbols, or "Aa" and "Ab," respectively. The cone-shaped reflection nebula R1 extends to $8''$ northeast from its illuminating source Haro 6-5 B. The dashed lines in the top panel indicate the straight edge of the dark i cloud suggested by Krist et al. (1998). The FOVs are $36''.3 \times 49''.4$ in the top panel and $18''.8 \times 22''.6$ in the bottom panel. North is up and east is to the left.

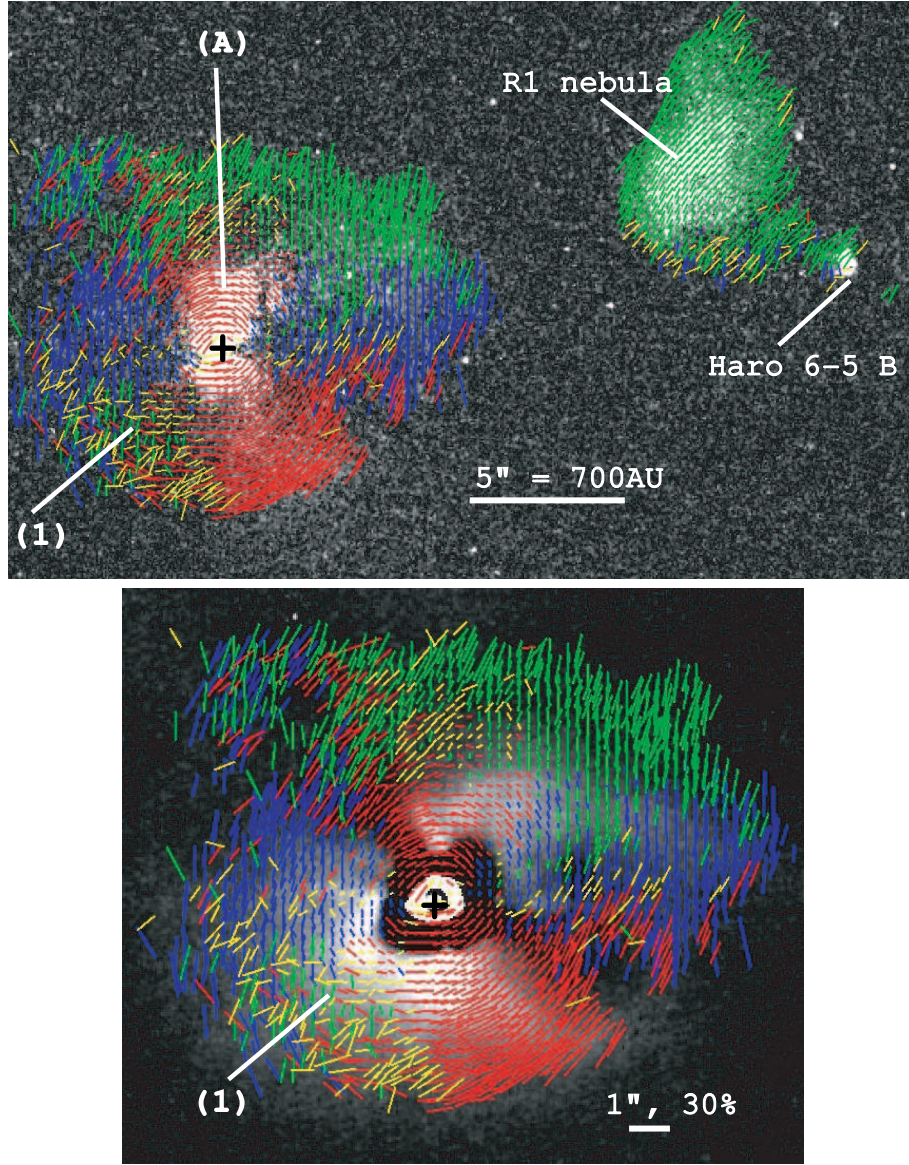


Fig. 3. The F606W-band polarized intensity image (*top*) and *H*-band coronagraphic image (*bottom*; same as Fig. 1) with the F606W-band polarization vectors. The vectors are $0''.25 \times 0''.25$ binned polarization vectors and are delineated by intensities above 3σ in each polarized image. The vectors are also classified as follows: $\theta_{\text{centroA}} < 30^\circ$ and $\theta_{\text{centroB}} > 30^\circ$ (*red*), $\theta_{\text{centroA}} < 30^\circ$ and $\theta_{\text{centroB}} < 30^\circ$ (*blue*), $\theta_{\text{centroA}} > 30^\circ$ and $\theta_{\text{centroB}} < 30^\circ$ (*green*), $\theta_{\text{centroA}} > 30^\circ$ and $\theta_{\text{centroB}} > 30^\circ$ (*yellow*). θ_{centroA} and θ_{centroB} are defined as the deviation from the centro-symmetric polarization patterns with respect to the FS Tau binary and Haro 6-5 B, respectively (see text). The polarization patterns are broadly centro-symmetric around the circumbinary disk, resulting from illumination by the FS Tau binary. "A" represents the local peak in the disk. The polarization vector is non-centro-symmetric around the *H*-band bright portion of the disk ("1"). The FOV is $19''.0 \times 30''.6$ in the top image and $13''.8 \times 16''.5$ in the bottom image. North is up and east is to the left.

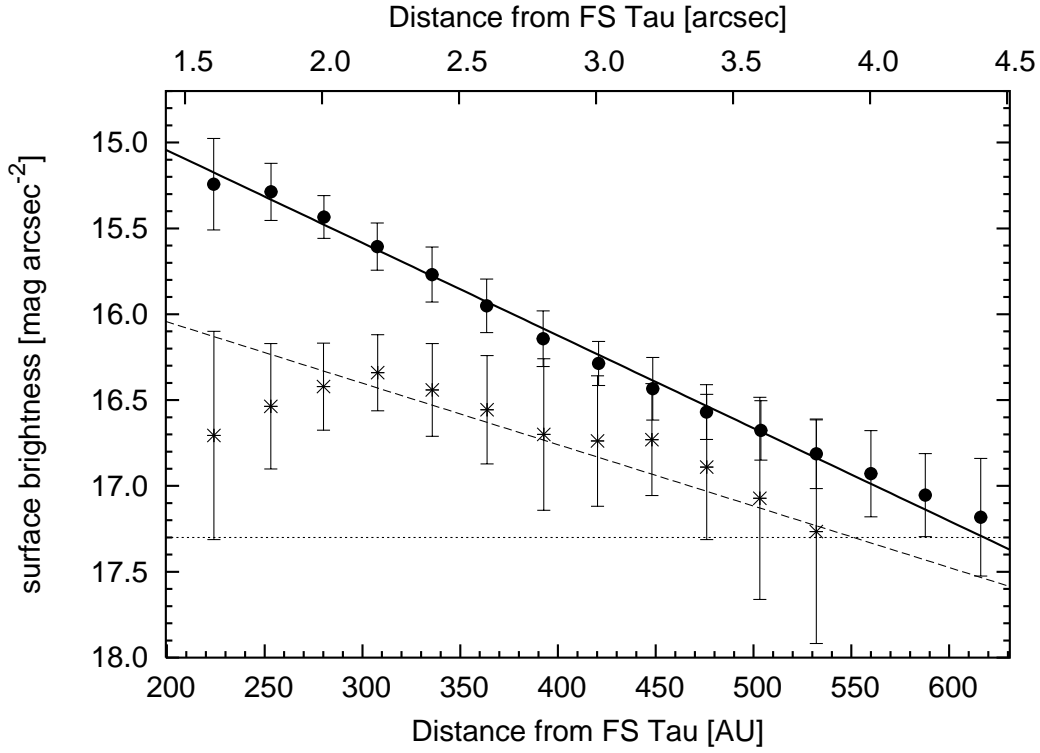


Fig. 4. The H -band surface brightness profile of the southeast (filled circle; P.A. = 93° to 175°) and northwest (asterisk; P.A. = 280° to 355°) sides of the binary. The brightnesses are averaged in a $0''.2 \times 0''.2$ aperture at $r = 220 - 630$ AU. The error bars represent standard deviations. The solid line represents a $r^{-1.9 \pm 0.1}$ power-law, and the dashed line represents a $r^{-1.5 \pm 0.3}$ power-law. The limiting magnitude of the observations ($17.3 \text{ mag arcsec}^{-2}$) is shown by the horizontal dotted line.

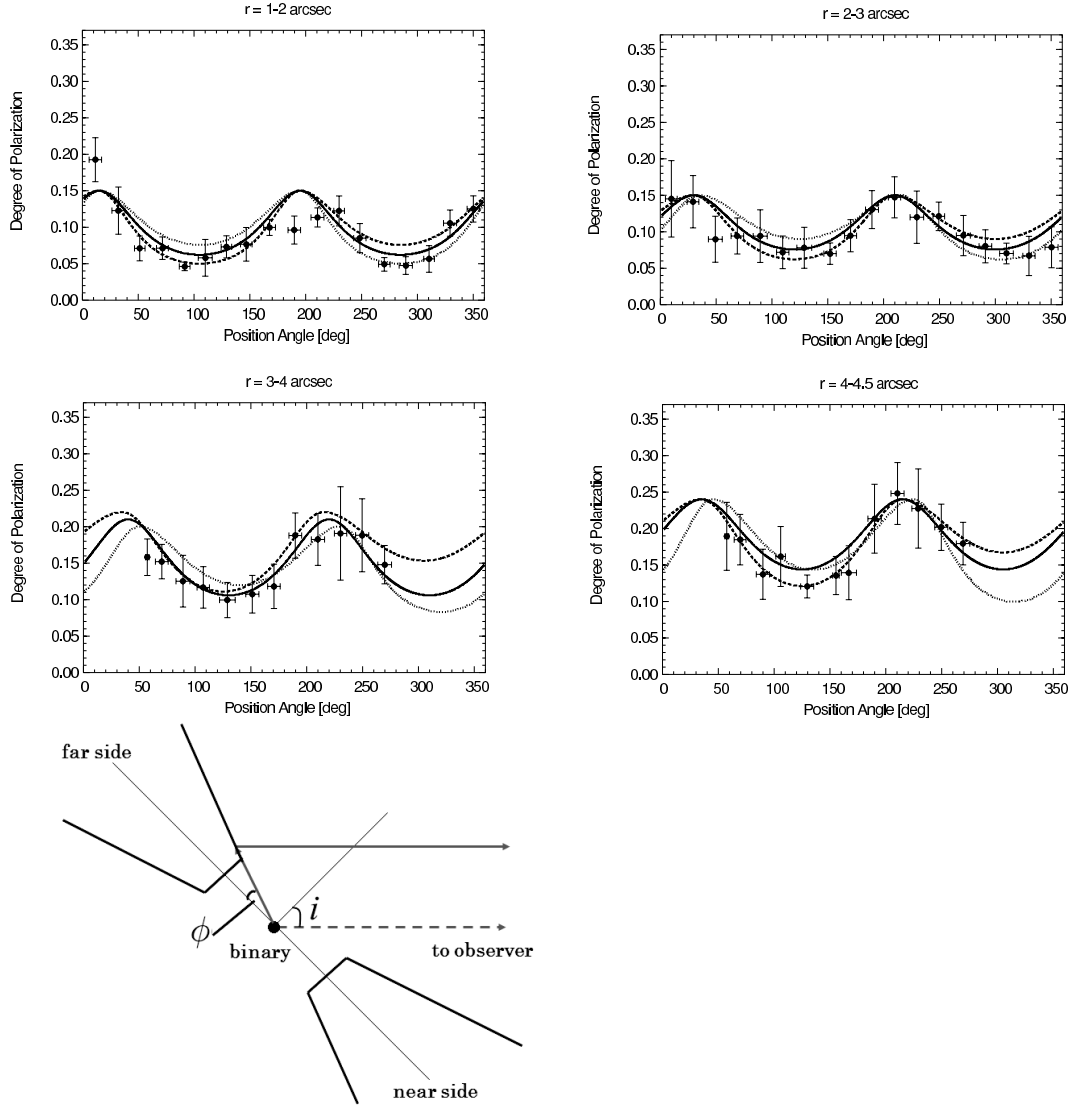


Fig. 5. The azimuthal polarization profiles for various distances from the binary, starting from the top left ($r = 1 - 2''$) and ending at the bottom right ($r = 4 - 4.5''$). The observed polarizations with $\theta_{\text{centroA}} < 30^\circ$ are applied to exclude the polarization due to multiple scattering events in the circumbinary disk. The observed polarizations in the $r > 3''$ north (P.A. = 280° to 55°) are not shown due to the contamination of the light from Haro 6-5 B. The solid curves represent the best match of the flat ($\phi = 0^\circ$) circumbinary disk model. The dashed curves represent the best match of the flared ($\phi = 5^\circ$) disk, where the southeast side corresponds to the near side. The dotted curves are the best match of the flared ($\phi = 5^\circ$) disks, where the northeast side is the near side. These χ^2 are shown in Table 1. " ξ " is the P.A. of the disk major axis, which is perpendicular to the plane of the bottom left panel. " i " is the disk inclination, and ϕ is the flared angle. No data are shown at $r < 1''$ due to the large uncertainty.

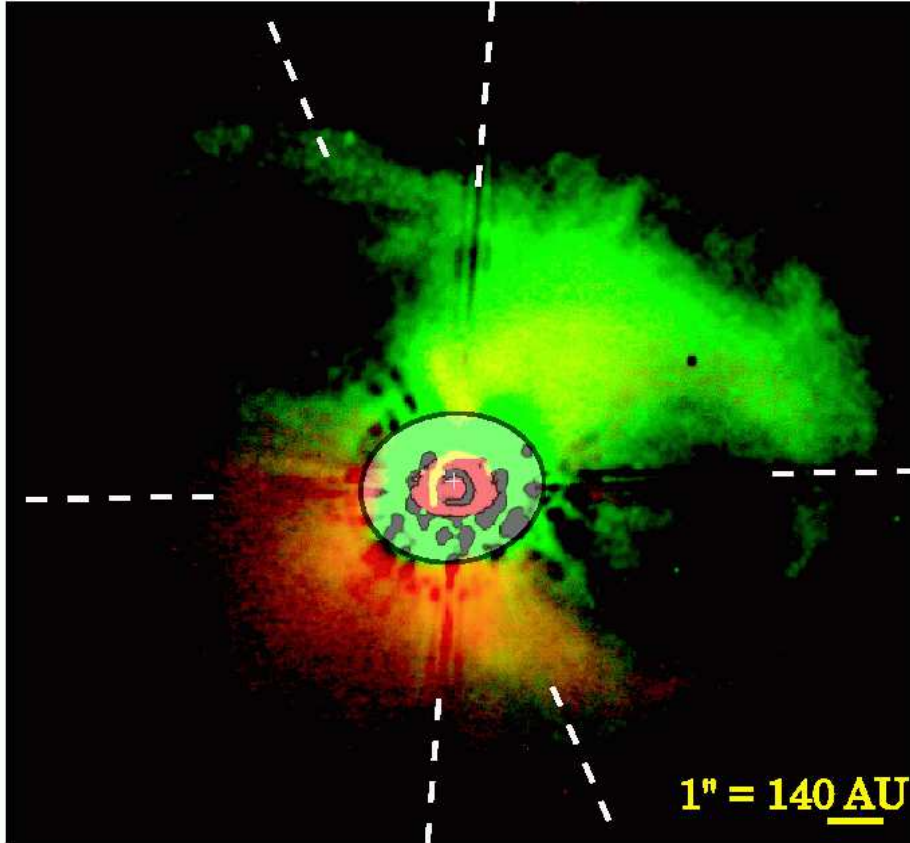


Fig. 6. The F606W–*H* color image of the FS Tau binary. The hatched ellipse marks the artifact region caused by the PSF-subtraction in both the F606W-band (*green*) and *H*-band images (*red*). The directions of the spider pattern are indicated by dashed lines. The FOV is $16''.5 \times 17''.5$. North is up and east is to the left.

Table 1. Best fit parameters for the circumbinary disk. ξ : the P.A. of the disk major axis; i : the disk inclination; ϕ : the flared angle.

Distance	ξ	i	ϕ	χ^2
[arcsec]	[deg]	[deg]	[deg]	
Flat Disk				
1 – 2	15	40	0	1.1
2 – 3	30	35	0	2.1
3 – 4	40	35	0	1.7
4 – 4.5	35	30	0	0.9
Flared Disk (SE)*				
1 – 2	15	40	5	1.2
2 – 3	30	35	5	2.3
3 – 4	35	30	5	1.7
4 – 4.5	35	30	5	0.8
Flared Disk (NW)*				
1 – 2	15	40	5	1.5
2 – 3	35	35	5	2.4
3 – 4	50	35	5	2.0
4 – 4.5	45	35	5	1.0

* The near side of the flared disk corresponds to the southeast (SE) or northwest (NW) sides.